CHEMISTRY OF MATERIALS

ARTICLE

pubs.acs.org/cm

Benzotrithiophene Co-polymers with High Charge Carrier Mobilities in Field-Effect Transistors

Bob C. Schroeder,[†] Christian B. Nielsen,[*,†] Young Ju Kim,[‡] Jeremy Smith,[§] Zhenggang Huang,[†] James Durrant,[†] Scott E. Watkins,[#] Kigook Song,[‡] Thomas D. Anthopoulos,[§] and Iain McCulloch[†]

[†]Department of Chemistry and Centre for Plastic Electronics, Imperial College London, London SW7 2AZ, United Kingdom

[‡]Kyung Hee University, Yongin, Gyeonggi-do 446-701, Korea

[§]Department of Physics and Centre for Plastic Electronics, Imperial College London, London SW7 2AZ, United Kingdom

[#]CSIRO Materials Science and Engineering, VIC 3169, Victoria, Australia

Supporting Information

ABSTRACT: The successful design and synthesis of two novel benzo[1,2-b:3,4-b′:5,6-d′]trithiophene-containing polymers is presented. The planar benzotrithiophene core induces strong aggregation effects in alternating co-polymers with both thiophene and thieno[3,2-b]thiophene. Co-monomer choice is found to play a crucial role in determining the backbone conformation, the interchain interactions, and the polymer solubility. Despite molecular disorder introduced by a branched solubilizing alkyl chain and a regiorandom polymerization of the asymmetric benzotrithiophene unit, these co-polymers exhibit hole mobilities as high as 0.24 $cm^2/(V\ s)$.

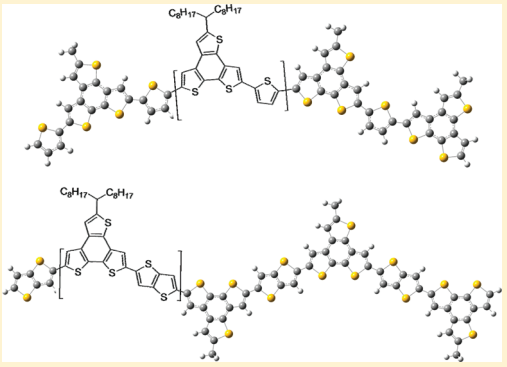

KEYWORDS: transistors, hole mobility, benzotrithiophene, conjugated polymers

1. INTRODUCTION

Since the discovery of the transistor effect in 1947, the development of suitable materials has been almost exclusively focused on inorganic semiconductors; however, during the last decades, a lot of effort has been put into the development of organic semiconductors and their performances are increasing rapidly.[1,2] Despite all the progress made so far, the electronic properties of organic semiconductors have not yet achieved the values of inorganic semiconductors; but this lack of performance is compensated by the versatile processability. Organic semiconducting materials can be processed using inexpensive solution-based manufacturing techniques, such as spin coating, inkjet printing, or roller casting, which allows the fabrication of large-area, flexible, and lightweight devices. In order to benefit from the processing versatility of semiconducting polymers and to establish them as cost-efficient alternatives to inorganic semiconductors, the electronic properties of organic semiconductors must be improved.

Herein, we report the synthesis of two new semiconducting polymers based on our newly developed benzo[1,2-b:3,4-b′:5,6-d′]trithiophene (BTT) moiety for organic field-effect transistor (OFET) applications.[3] The BTT unit is designed with inspiration from benzo[1,2-b:4,5-b′]dithiophene by fusing three thiophene units to a central benzene core instead of two, in order to increase the size and electronic density of the aromatic building block. The large BTT core is planar and should allow for very effective intermolecular packing in the solid state. By co-polymerizing the BTT unit with thiophene (T) and thieno[3,2-b]thiophene (TT) units, we show that highly ordered and partially crystalline polymer films can be obtained, which display good charge carrier mobilities when employed as semiconducting materials in OFETs.

2. EXPERIMENTAL SECTION

2.1. Materials and Methods. All chemicals were purchased from commercial suppliers, unless specified otherwise. ^1H NMR and ^{13}C NMR spectra were recorded on a Bruker Model 400 spectrometer in $CDCl_3$ solution at 298 K, unless stated otherwise. Number-average and weight-average molecular weights (M_n and M_w, respectively) were determined with an Agilent Technologies 1200 series gel permeation chromatography (GPC) system in chlorobenzene at 80 °C, using two photoluminescent mixed B columns in series, and calibrated against narrow polydispersity polystyrene standards. Electrospray and electron ionization mass spectrometry were performed with a Thermo Electron Corporation Model DSQIIc system and a Micromass AutoSpec Premier mass spectrometer, respectively. Ultraviolet−visible light (UV−vis) absorption spectra were recorded on a Shimadzu Model UV-1601 UV−vis spectrometer. Column chromatography was carried out on silica gel (for flash chromatography, from VWR Scientific). Microwave experiments were performed in a Biotage initiator V 2.3. Photoelectron spectroscopy in air (PESA) measurements were recorded with a Riken Keiki Model AC-2 PESA spectrometer with a power setting of 5 nW and a power number of 0.5. Atomic force microscopy (AFM)

Received: June 6, 2011
Revised: August 2, 2011
Published: August 16, 2011

was performed on a Agilent Technology Model 5500 AFM system in tapping mode. Polarized optical microscopy (POM) was performed with a Nikon Model LV100 microscope. X-ray diffraction (XRD) measurements were carried out with a Panalytical Model X'Pert PRO MRD diffractometer equipped with a nickel-filtered Cu $K\alpha_1$ beam and a X'Celerator detector, using a current of I = 40 mA and an accelerating voltage of U = 40 kV. Organic field-effect transistors (OFETs) were prepared using bottom gate, top contact test structures. Highly p-doped silicon wafers with 400 nm of thermally grown SiO_2 were used as substrates and the silicon dioxide dielectric layer was hydrophobically modified by exposure in an oxygen plasma for 5 min and immersion in a 20 mM toluene solution of octadecyltrichlorosilane (OTS) at room temperature for 1 h. Films were spin-cast at 1000 rpm from polymer solutions of 5 mg/mL in chlorobenzene at 80 °C. After casting, films were heated to 100 °C for 10 min and then further heated to 200 °C for 10 min for the annealing. For the source and drain electrodes, 70 nm of thermally evaporated gold was used. The carrier mobility of the films was assessed by measuring transfer curves in saturation (V_{DS} = −60 V), using a Keithley Model 4200 semiconductor parameter analyzer in a nitrogen atmosphere. The saturation mobility was determined by fitting a linear relationship of the square root of the drain current to gate potential in the range of −40 V to −60 V gate potential. The saturation mobility was measured on three devices.

2.2. Monomer Synthesis. *2.2.1. 2,3-Dibromo-5-nonanoylthiophene (**1**).* To an ice-cooled solution of 2,3-dibromothiophene (25.24 g, 104.3 mmol) and nonanoyl chloride (22.0 mL, 117 mmol) in dichloromethane (200 mL) was added aluminum chloride (18.3 g, 137 mmol), in a portion-wise manner, for 15 min. The reaction mixture was stirred for 2 h and then quenched with ice-cold hydrochloric acid (2 M, 400 mL). The quenched reaction mixture was extracted with dichloromethane and dried over anhydrous magnesium sulfate; removal of the solvent afforded the crude product, which was extracted with hexane and subsequently concentrated to afford the title compound (38.2 g, 100 mmol, 96% yield) as a brown oil, which was used in the next step without further purification. ^{1}H NMR (400 MHz, $CDCl_3$): δ 7.44 (s, 1H), 2.78 (t, 2H), 1.69 (m, 2H), 1.26 (m, 10H), 0.85 (t, 3H). ^{13}C NMR (100 MHz, $CDCl_3$): δ 191.92, 144.78, 133.73, 121.43, 115.07, 38.77, 32.00, 29.52, 29.43, 29.31, 24.67, 22.84, 14.30. MS: m/z 380 (M^+), 282 (100, $M-C_7H_{14}$). HRMS (EI): m/z calcd for $C_{13}H_{18}Br_2OS$ (M^+), 379.9445; found, 379.9450.

*2.2.2. 5-Nonanoyl-2,3-bis(3-thienyl)thiophene (**2**).* A suspension of **1** (13.37 g, 34.99 mmol), thiophene-3-boronic acid (10.49 g, 81.98 mmol) and sodium carbonate (42 g, 0.40 mol) in toluene (110 mL), ethanol (110 mL), and water (110 mL) was degassed by bubbling with argon for 2 h. Tetrakis(triphenylphosphine)palladium(0) (1.05 g, 0.909 mmol) then was added and the reaction mixture was heated to reflux for 24 h. The reaction mixture was quenched with water, extracted with diethyl ether, dried over anhydrous magnesium sulfate, and concentrated to afford the crude product. Purification by column chromatography (silica, toluene) and subsequent recrystallization (toluene/methanol) afforded the title compound (10.81 g, 27.82 mmol, 80% yield) as a pale yellow solid. ^{1}H NMR (400 MHz, $CDCl_3$): δ 7.66 (s, 1H), 7.30 (dd, J = 5.0, 3.0 Hz, 1H), 7.27 (m, 2H), 7.21 (dd, J = 3.0, 1.3 Hz, 1H), 6.99 (m, 2H), 2.86 (t, 2H), 1.74 (m, 2H), 1.26 (m, 10H), 0.86 (t, 3H). ^{13}C NMR (100 MHz, $CDCl_3$): δ 193.60, 141.51, 141.26, 136.22, 134.37, 134.06, 134.02, 128.17, 127.91, 126.33, 126.00, 124.57, 123.36, 39.29, 32.02, 29.58, 29.57, 29.35, 25.11, 22.85, 14.30. MS: m/z 388 (M^+), 290 (100, $M-C_7H_{14}$). HRMS (ESI-TOF): m/z calcd for $C_{21}H_{25}OS_3^+$ (MH^+), 389.1062; found, 389.1054.

*2.2.3. 5-Nonanoylbenzo[1,2-b:3,4-b′:5,6-d″]trithiophene (**3**).* To an ice-cooled solution of **2** (7.0 g, 18.0 mmol) in anhydrous dichloromethane (500 mL) was added boron trifluoride diethyl etherate (3.6 mL, 28.8 mmol), after which 2,3-dichloro-5,6-dicyano-1,4-benzoquinone (6.2 g, 27.3 mmol) was added, in a portion-wise manner, for 10 min. The reaction mixture was allowed to warm to room temperature overnight. After 48 h, the reaction was subsequently quenched via the addition of zinc (10.6 g, 162 mmol) and methanol (250 mL). After stirring overnight, the reaction mixture was filtered, washed with water, dried over anhydrous magnesium sulfate, and concentrated to afford the crude product. Purification by column chromatography (silica, toluene) and subsequent recrystallization (ethanol) afforded the title compound (3.92 g, 10.16 mmol, 56% yield) as a yellow-orange solid. ^{1}H NMR (400 MHz, $CDCl_3$): δ 8.19 (s, 1H), 7.65 (d, J = 5.3 Hz, 1H), 7.54 (d, J = 5.4 Hz, 1H), 7.48 (d, J = 5.3 Hz, 1H), 7.47 (d, J = 5.4 Hz, 1H), 3.01 (t, 2H), 1.80 (m, 2H), 1.27 (m, 10H), 0.87 (t, 3H). ^{13}C NMR (100 MHz, $CDCl_3$): δ 194.85, 142.20, 136.29, 133.63, 133.35, 132.32, 131.75, 131.25, 127.20, 125.60, 125.40, 122.79, 122.64, 39.57, 32.05, 29.65, 29.61, 29.39, 25.01, 22.87, 14.32. MS: m/z 386 (M^+), 288 (100, $M-C_7H_{14}$). HRMS (ESI-TOF): m/z calcd for $C_{21}H_{23}OS_3$ (MH^+), 387.0906; found, 387.0912.

*2.2.4. 5-((1-Hydroxy-1-octyl)nonyl)benzo[1,2-b:3,4-b′:5,6-d″]trithiophene (**4**).* Compound **3** (5.6 g, 14.5 mmol) was dissolved in diethyl ether (270 mL) and the solution was cooled to 0 °C before a 2 M diethyl ether solution of octylmagnesium bromide (10.2 mL, 20.4 mmol) was added dropwise. The resulting solution was stirred at 0 °C for 1 h and then slowly warmed to room temperature, before it was heated to reflux overnight. The reaction mixture was cooled to room temperature and quenched with 200 mL of saturated ammonium chloride solution. The aqueous phase was extracted twice with diethyl ether; the combined organic phases were dried with magnesium sulfate and the solvent was evaporated under reduced pressure. The crude product was purified by column chromatography (silica, toluene) to afford compound **2** as a pale yellow solid (5.83 g, 11.65 mmol, 80% yield). ^{1}H NMR (400 MHz, $CDCl_3$): δ 7.70 (d, J = 5.3 Hz, 1H), 7.56 (d, J = 5.4 Hz, 1H), 7.52 (s, 1H), 7.47 (d, J = 5.4 Hz, 1H), 7.46 (d, J = 5.3 Hz, 1H), 2.16 (s, 1H), 1.94 (m, 4H), 1.41 (m, 4H), 1.22 (m, 20H), 0.84 (t, 6H). ^{13}C NMR (100 MHz, $CDCl_3$): δ 151.74, 132.89, 132.75, 131.67, 131.50, 129.25, 128.44, 125.18, 124.46, 122.97, 122.49, 118.30, 77.43, 43.75, 32.05, 30.14, 29.69, 29.46, 23.80, 22.84, 14.30. MS: m/z 482 ($M-H_2O$), 286 (100, $M-H_2O$ $-C_{14}H_{28}$). HRMS (ESI-TOF): m/z calcd for $C_{29}H_{39}S_3$ (MH^+-H_2O), 483.2208; found, 483.2222.

*2.2.5. 5-(1-Octylnonyl)benzo[1,2-b:3,4-b′:5,6-d″]trithiophene (**5**).* To lithium aluminum hydride (4.67 g, 123 mmol) was added 330 mL of anhydrous diethyl ether via cannulation. Aluminum chloride (6.26 g, 47 mmol) was carefully added as a solid to the solution, which was then cooled down to 0 °C with an ice-bath. **4** (5.6 g, 11.18 mmol) was dissolved in 100 mL of anhydrous diethyl ether and then added by cannulation to the lithium aluminum hydride solution. After complete addition, the ice-bath was removed and the reaction was allowed to warm to room temperature. After 36 h, the reaction mixture was poured in 1.5 L of ice, preliminary acidified with 60 mL of concentrated hydrochloric acid. Potassium hydroxide was added under stirring to break up the emulsion. The crude compound was extracted with diethyl ether; the combined organic phases were dried with magnesium sulfate and concentrated to a yellow oil under reduced pressure. The crude product was purified by column chromatography (silica, cyclohexane) to yield the title compound (4.34 g, 8.95 mmol, 80% yield) as a yellow solid. ^{1}H NMR (400 MHz, $CDCl_3$): δ 7.69 (d, J = 5.3 Hz, 1H), 7.55 (d, J = 5.3 Hz, 1H), 7.47 (d, J = 5.3 Hz, 1H), 7.46 (d, J = 5.3 Hz, 1H), 7.40 (s, 1H), 2.97 (m, 1H), 1.71 (m, 4H), 1.21 (m, 24H), 0.84 (t, 6H). ^{13}C NMR (100 MHz, $CDCl_3$): δ 150.58, 132.79, 132.58, 131.87, 131.01, 130.96, 129.92, 125.00, 124.24, 123.03, 122.50, 119.36, 42.63, 38.26, 32.08, 29.87, 29.71, 29.52, 27.77, 22.86, 14.32. MS: m/z 484 (M^+), 259 (100, $M-C_{16}H_{33}$). HRMS (EI): m/z calcd for $C_{29}H_{40}S_3$ (M^+), 484.2293; found, 484.2292.

*2.2.6. 2,8-Dibromo-5-(1-octylnonyl)benzo[1,2-b:3,4-b′:5,6-d″]trithiophene (**6**).* To a solution of **5** (324 mg, 0.668 mmol) in anhydrous tetrahydrofuran (30 mL) cooled to −78 °C was added *tert*-butyllithium (1.7 M in pentane, 2.0 mL, 3.4 mmol) dropwise during 10 min. The reaction mixture was stirred for 2 h at −78 °C, warmed to 0 °C for 30 min, and then cooled to −78 °C again, whereupon 1,2-dibromotetrachloroethane

dx.doi.org/10.1021/cm2015884 |*Chem. Mater.* 2011, 23, 4025–4031

Scheme 1. Synthesis of the BTT Precursor

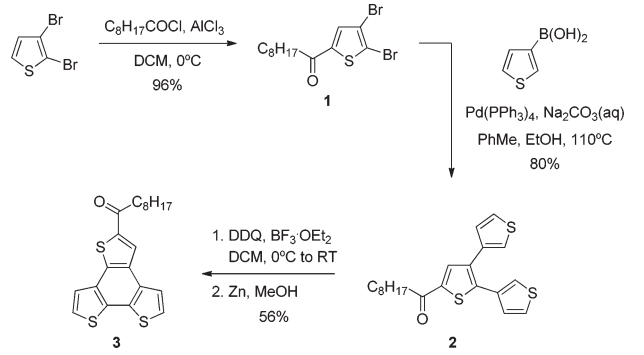

(1.20 g, 3.68 mmol) was added and the reaction mixture was allowed to warm to room temperature overnight. The reaction mixture was quenched with water, extracted with diethyl ether, dried over anhydrous magnesium sulfate and concentrated to afford the crude product. Washing with methanol and subsequent column chromatography (silica, petrol ether) afforded the title compound (345 mg, 0.537 mmol, 80% yield) as a white solid. ^{1}H NMR (400 MHz, $CDCl_3$): δ 7.61 (s, 1H), 7.46 (s, 1H), 7.26 (s, 1H), 2.94 (s, 1H), 1.67 (m, 4H), 1.20 (m, 24H), 0.83 (t, 6H). ^{13}C NMR (100 MHz, $CDCl_3$): δ 151.56, 132.22, 132.12, 131.64, 130.70, 130.31, 129.53, 125.88, 125.26, 118.96, 113.81, 113.01, 42.57, 38.13, 32.07, 29.83, 29.70, 29.51, 27.73, 22.87, 14.31. MS: m/z 640 (M^+), 415 (100, M−$C_{16}H_{33}$). HRMS (EI): m/z calcd for $C_{29}H_{38}Br_2S_3$ (M^+), 640.0502; found, 640.0497.

2.3. Polymer Synthesis. *2.3.1. Poly[(5-(1-octylnonyl)benzo-[1,2-b:3,4-b′:5,6-d″]trithiophene-2,8-diyl)-alt-co-(thiophene-2,5-diyl)] (BTT-T).* Monomer **6** (150 mg, 0.233 mmol) was added, together with 2,5-bis(trimethylstannyl)thiophene (96 mg, 0.233 mmol) and tetrakis-(triphenylphosphine)palladium (13.49 mg, 12 μmol), to a microwave vial. After the vial was sealed, 0.8 mL of anhydrous chlorobenzene were added and the resulting solution was degassed with argon, before it was subjected to the following heating conditions in a microwave reactor: 100 °C for 2 min, 120 °C for 2 min, 140 °C for 10 min, and finally 160 °C for 30 min. After reaction, the crude polymer was precipitated in methanol and then further purified by Soxhlet extractions with acetone, cyclohexane, THF, and chloroform, each for 24 h. Remaining palladium residues were removed by treating a polymeric chlorobenzene solution with an aqueous sodium diethyldithiocarbamate solution for 1 h at 60 °C under vigorous stirring. Afterward, the organic phase was separated from the aqueous phase and washed several times with water. The polymeric solution was concentrated under reduced pressure and precipitated into methanol. BTT-T (66 mg, 0.11 mmol) was recovered as a dark red solid. GPC (chlorobenzene): M_n = 16.6 kDa, M_w = 48.2 kDa, PDI = 2.90. ^{1}H NMR (500 MHz, o-$C_6D_4Cl_2$, 60 °C): δ 7.8−6.7 (br, 5H), 3.6−3.1 (br, 1H), 2.8−0.6 (br, 34H).

2.3.2. Poly[(5-(1-octylnonyl)benzo[1,2-b:3,4-b′:5,6-d″]trithiophene-2,8-diyl)-alt-co-(thieno[3,2-b]thiophene-2,5-diyl)] (BTT-TT). A 5-mL microwave vial was charged with monomer **6** (150 mg, 0.233 mmol), 2,5-bis(trimethylstannyl)thieno[3,2-b]thiophene (109 mg, 0.233 mmol), and tetrakis(triphenylphosphine)palladium (13.49 mg, 12 μmol). The vial was sealed and 0.8 mL of anhydrous chlorobenzene was added. The obtained solution was bubbled with argon prior to submitting the reaction vessel to the following heating conditions in a microwave reactor: 2 min at 100 °C, 2 min at 120 °C, 20 min at 140 °C, and 5 min at 160 °C. After cooling, the crude polymer solution was added dropwise to methanol. The formed precipitate was Soxhlet-extracted in acetone, cyclohexane, and chloroform. Residual palladium salts were removed by treating a polymeric chlorobenzene solution with an aqueous sodium diethyldithiocarbamate solution for 1 h at 60 °C under vigorous stirring. The organic phase was separated from the aqueous phase and washed several times with water. The polymeric solution was concentrated under reduced pressure and precipitated into methanol. BTT-TT (75 mg, 115 μmol) was recovered as a dark red solid. GPC (chlorobenzene): M_n = 6.2 kDa, M_w = 13.1 kDa, PDI = 2.11. ^{1}H NMR (500 MHz, o-$C_6D_4Cl_2$, 60 °C): δ 8.2−6.7 (br, 5H), 3.7−3.0 (br s, 1H), 2.7−0.6 (br, 34H).

Scheme 2. Synthesis of the BTT Monomer

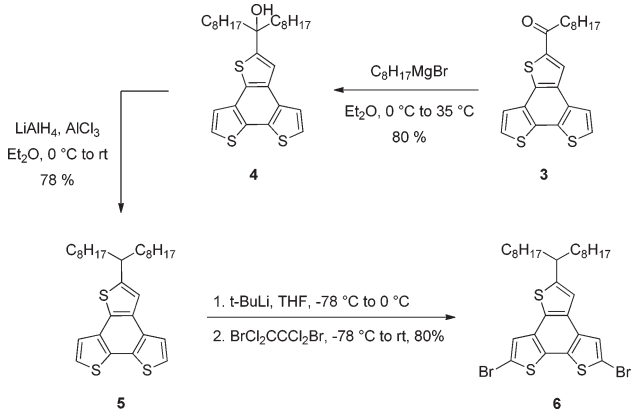

Scheme 3. Synthesis of the BTT Co-polymers

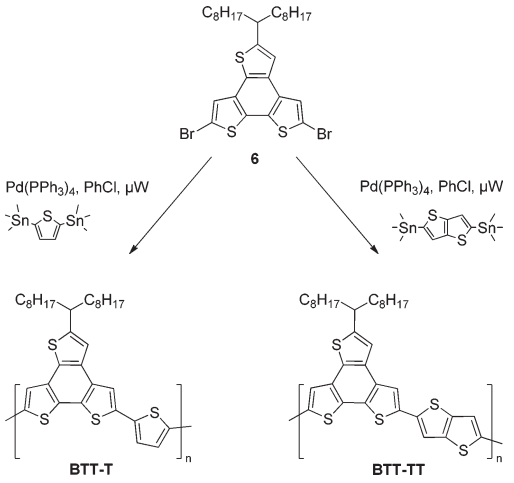

3. RESULTS AND DISCUSSION

3.1. Synthesis. The branched alkyl BTT core was obtained by extending our previously published synthetic pathway as outlined in Schemes 1 and 2.[3] Compound **3** was prepared in three steps from commercially available 2,3-dibromothiophene in an overall yield of 43% (Scheme 1), attaching first the solubilizing side chain by a Friedel−Crafts acylation, then two thiophene units by a Suzuki−Miyaura cross-coupling and finally assembling the BTT core by an oxidative Scholl-type ring closure. Compound **3** can be reduced to a linear alkyl-substituted BBT, but our initial studies revealed that even long (C16) linear alkyl chains provide limited solubility to this system. In order to improve the solubility of the BTT unit, a second octyl chain was therefore added to compound **3** via a Grignard reaction to obtain the corresponding tertiary alcohol (**4**) in an 80% yield (see Scheme 2). Compound **4**

dx.doi.org/10.1021/cm2015884 |*Chem. Mater.* 2011, 23, 4025–4031

Chart 1. Illustration of Regioregular-Type (Left) and Regiorandom-Type (Right) Connectivity for BTT Co-polymers

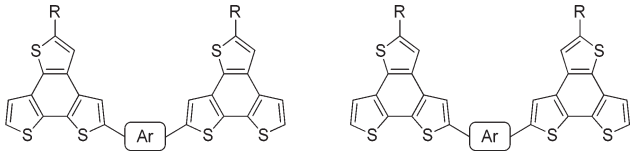

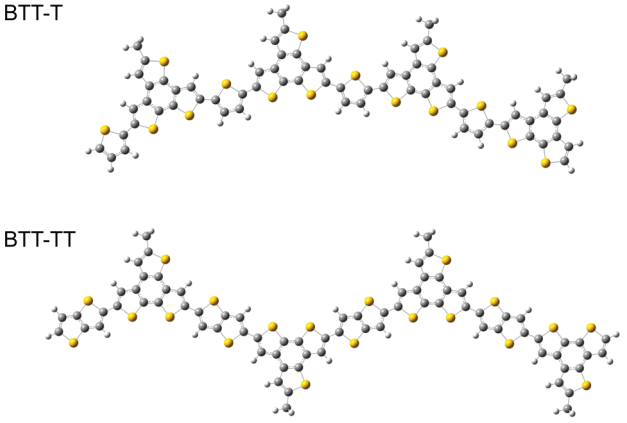

Figure 1. Minimum-energy conformations of tetramers of BTT-T (top) and BTT-TT (bottom) Gaussian-optimized at the B3LYP/6-31G* level.

was subsequently reduced with lithium aluminum hydride in the presence of aluminum chloride to give the branched and highly soluble alkyl BTT (**5**) in a good yield of 78%. Finally, compound **5** was selectively lithiated at the two free α-positions with *tert*-butyllithium and the resulting dilithiated species was quenched with 1,2-dibromotetrachloroethane to afford the 2,8-dibrominated BTT (**6**) in good yield (80%) and excellent purity.

Incorporating the branched alkyl BTT dibromide (**6**), the two new polymers shown in Scheme 3 were synthesized by Stille cross-couplings under microwave heating conditions, using trimethyltin-functionalized T and TT co-monomers, $Pd(PPh_3)_4$ was used as the catalyst, and chlorobenzene was used as the solvent. The crude polymers were precipitated in methanol and then further purified by Soxhlet extractions with acetone, cyclohexane, and chloroform. Palladium residues were removed by washing a polymeric chlorobenzene solution with an aqueous sodium diethyldithiocarbamate solution. The molecular weight achieved for BTT-T was M_n = 16.6 kg/mol (PDI = 2.90), whereas a lower molecular weight was achieved for the BTT-TT polymer (M_n = 6.2 kg/mol, PDI = 2.11). For BTT-TT, the polymerization was intentionally stopped at a rather low degree of polymerization by visually monitoring the viscosity of the reaction mixture, since all our efforts to increase the molecular weight further resulted in insoluble polymers.

Both polymers displayed good thermal stability with a 5% weight loss observed at 371 °C (BTT-TT) and 393 °C (BTT-T), respectively, when subjected to thermogravimetric analysis (TGA) (see Figure S11 in the Supporting Information). Differential scanning calorimetry (DSC) (see Figure S12 in the Supporting Information) did not show any thermal transitions for either of the two polymers.

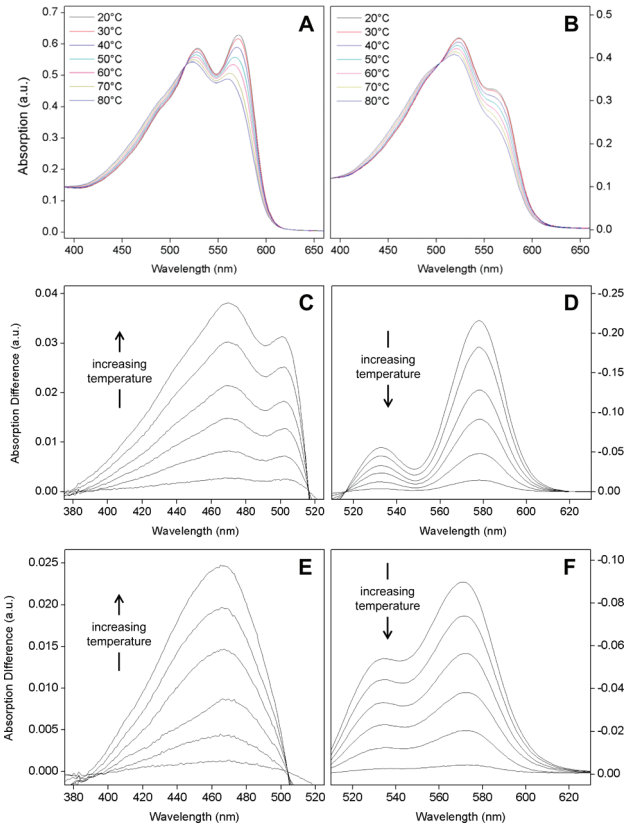

Figure 2. Temperature-dependent UV−vis absorption spectroscopy of (A) BTT-T and (B) BTT-TT in *o*-dichlorobenzene and difference spectra for (C and D) BTT-T and (E and F) BTT-TT used to deconvolute the absorption bands from fully solubilized material and aggregated species.

We emphasize that the polymer structures depicted in Scheme 3 are merely drawn in a regioregular fashion for simplicity; we have made no synthetic efforts to control the regiochemistry arising from the noncentrosymmetric nature of the BTT monomer caused by the asymmetric alkyl-bearing thiophene unit and, therefore, we expect the co-polymers to be regiorandomly connected, as illustrated in Chart 1.

The minimum-energy conformations of the tetramers of BTT-T and BTT-TT (see Figure 1) reveal several significant differences between the two systems. As the size of the co-monomer increases from T to TT, the intrachain separation—and, subsequently, the spatial density—of the alkyl-bearing BTT units obviously increases (from ∼12 Å for T to ∼15 Å for TT), giving rise to a decrease in polymer solubility. Moreover, as can be seen in Figure 1, the backbone of BTT-T is slightly curved with all alkyl groups facing the same side of the backbone, whereas BTT-TT orients in a planar zigzag conformation, preserving long-range linearity, with adjacent alkyl groups on opposite sides of the backbone. These factors will affect the degree of polymerization, as we have observed: compared to BTT-TT, BTT-T is more curved, less structured, and, hence, more soluble, which will support higher-molecular-weight chain growth during the polymerization. The conformational differences will also influence the solid-state packing, interchain interactions, and charge carrier mobility of these copolymers.[2c,4]

3.2. Optical Absorption. The UV−vis spectra of the two polymers in *o*-dichlorobenzene solution and as spin-cast thin

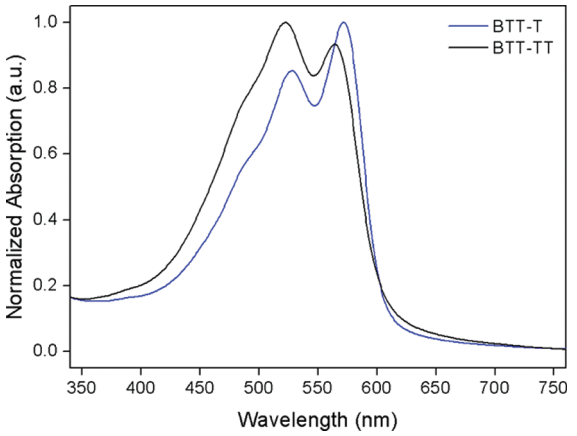

Figure 3. Normalized UV−vis absorption spectra of thin films of BTT-T and BTT-TT spin-cast from *o*-dichlorobenzene.

Table 1. Optical Properties and Experimental and Calculated Energy Levels of Polymers BTT-T and BTT-TT

			E_g (eV)		HOMO (eV)	
	λ_{max} (nm) soln[a]	λ_{max} (nm) film[b]	exp[c]	calc[d]	exp[e]	calc[d]
BTT-T	470, 501	528, 572	2.06	2.10	−5.09	−4.80
BTT-TT	465	522, 564	2.05	2.05	−5.04	−4.79

[a] Measured in dilute *o*-dichlorobenzene solution; values extracted from temperature-dependent studies. [b] Spin-coated from *o*-dichlorobenzene solution. [c] Estimated from the optical absorption onset. [d] Calculated with Gaussian using the B3LYP/6-31G* model. [e] Measured by UV-PESA.

films are depicted in Figures 2 and 3 and summarized in Table 1. In solution, they show multiple absorption features, most notably BTT-T, which has two well-defined peaks (at 529 and 573 nm), whereas the higher wavelength feature is reduced to a shoulder for BTT-TT. Temperature-dependent UV−vis (see Figures 2A and 2B) confirms that the polymers are aggregating in solution and a clear isosbestic point for both polymers further supports our hypothesis of an aggregate-to-solute conversion upon heating. Difference spectra from the temperature-dependent study are used to deconvolute the absorption bands from fully solubilized material (see Figures 2C and 2E) and from aggregated species (see Figures 2D and 2F). We observe spectral broadening and a slight red-shift of the solution absorption maximum (Table 1), when comparing BTT-T to BTT-TT, most likely as a consequence of the increase in molecular weight.

In the solid state, the polymers display one strong absorption feature in the 450−600 nm region with a low-wavelength shoulder and two distinct peaks at ∼520−530 nm and ∼560−570 nm, as illustrated in Figure 3. Again, the absorption features for BTT-T are slightly red-shifted, relative to BTT-TT; this is an observation that, most likely, can be ascribed to the difference in molecular weight between the two polymers. The observed optical band gaps of ∼2.05 eV determined from the absorption onset are in good agreement with quantum-chemical calculations (B3LYP/6-31G*), despite the variance in molecular weights observed for the polymers.

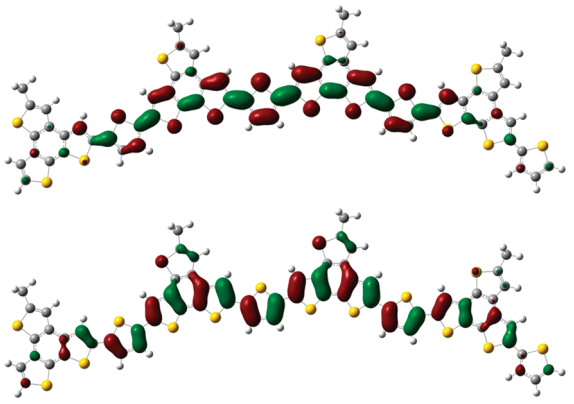

Figure 4. LUMO (top) and HOMO (bottom) distributions for the minimum-energy conformation of a tetramer of BTT-T Gaussian-optimized at the B3LYP/6-31G* level.

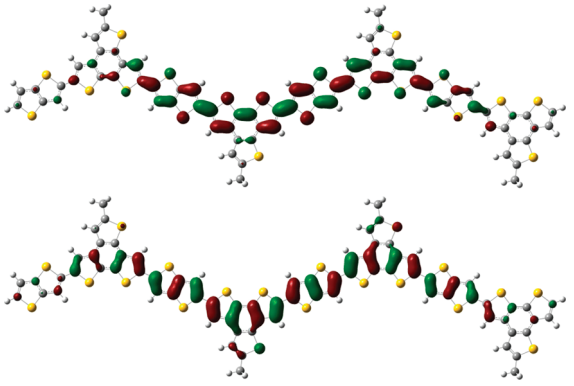

Figure 5. LUMO (top) and HOMO (bottom) distributions for the minimum-energy conformation of a tetramer of BTT-TT Gaussian-optimized at the B3LYP/6-31G* level.

The highest occupied molecular orbital (HOMO) energy levels of the polymers were measured by photoelectron spectroscopy in air (UV-PESA; see Table 1) and values of −5.09 and −5.04 eV were found for BTT-T and BTT-TT, respectively. The lowest unoccupied molecular orbital (LUMO) energy levels were subsequently estimated from the optical band gaps and the HOMO levels; values of −3.03 eV for BTT-T and −2.99 eV for BTT-TT were obtained. We stress that the observed tendencies for aggregation imply that the thin-film morphology of these materials can vary greatly with processing conditions (choice of casting technique, solvent, temperature, and concentration). Since the morphology can affect both UV-PESA and UV−vis measurements, the values obtained for the frontier-orbital energy levels must be regarded as estimated values. The theoretical computations furthermore predict the HOMOs and LUMOs to be delocalized over the entire conjugated backbone for both systems (see Figures 4 and 5). The HOMOs are predominantly aromatic in nature, whereas the LUMOs mainly are of quinoidal character for both polymers. The distribution of the HOMO over a large unit especially bodes well for efficient intermolecular charge transport for the two BTT-containing co-polymers.

3.3. Field-Effect Transistor Devices. Using a bottom-gate/top-contact transistor device architecture, the polymers were deposited onto octadecyltrichlorosilane-treated Si/SiO_2 substrates by spin-coating from chlorobenzene and Au electrodes

dx.doi.org/10.1021/cm2015884 |*Chem. Mater.* 2011, 23, 4025–4031

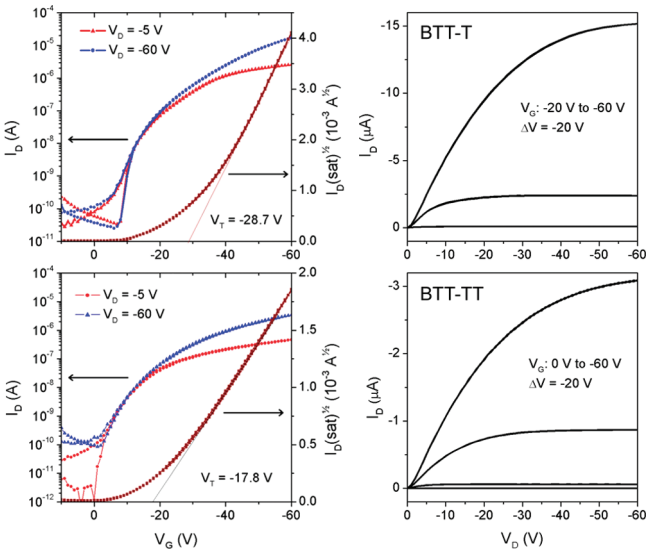

Figure 6. Transfer (left) and output (right) characteristics of a BTT-T FET device (top) and a BTT-TT FET device (bottom) spin-coated from chlorobenzene (5 mg/mL) and annealed at 200 °C for 10 min (L = 50 μm, W = 1.0 mm).

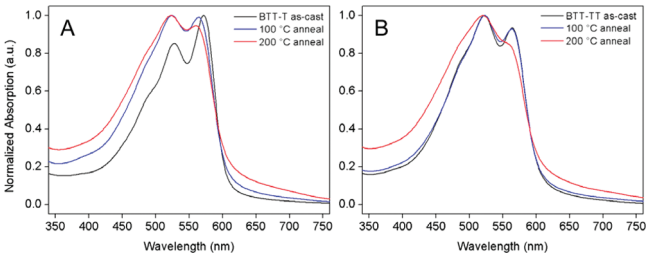

Figure 7. UV−vis absorption spectra of as-cast and thermally annealed thin films of (A) BTT-T and (B) BTT-TT.

were deposited on top by thermal evaporation. After annealing at 200 °C, the polymer films showed hole mobilities as high as 0.24 cm^2/(V s) for BTT-T (average of 0.21 for three devices, on/off ratio of ~10^6) and 0.025 cm^2/(V s) for BTT-TT (average of 0.022 for three devices, on/off ratio of ~10^4). We mainly attribute the one-order-of-magnitude-larger charge carrier mobility of BTT-T, compared to BTT-TT, to the 3-fold increase in molecular weight, which is most likely caused by the higher degree of curvature, and, thus, solubility, of the polymer backbone, as discussed above. On the other hand, the mobility of BTT-TT is surprisingly high for a fairly polydisperse sample with an average degree of polymerization of only ~10 repeat units. This highlights the fact that even short oligomeric chains of BTT-TT are able to pack favorably for charge transport in the solid state. Judging from the energy-optimized structures in Figure 1, we expect BTT-TT to hold great promise for further optimization, in relation to OFET characteristics, if the difficulties with solubility and processability can be overcome by side chain optimization. The BTT-T and BTT-TT polymers exhibited good transfer curves with negligible hysteresis, and the output curves showed only slight nonlinearity (see Figure 6) at low source-drain voltages. The low-lying HOMO levels of these polymers (Table 1), although making hole injection more difficult, promote good ambient stability,

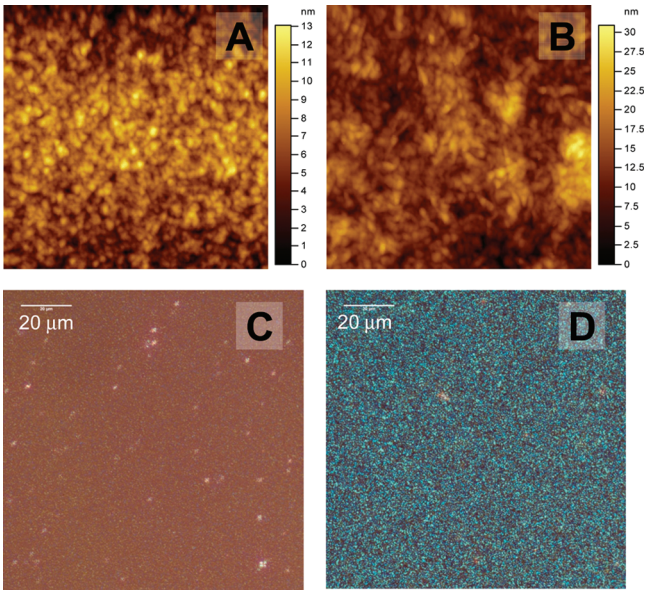

Figure 8. Close-contact atomic force microscopy (AFM) topography images (2.0 μm × 2.0 μm) of spin-cast and 200 °C annealed films of (A) BTT-T and (B) BTT-TT and polarized optical microscopy (POM) images (50× magnification, reflection mode) for (C) BTT-T and (D) BTT-TT.

which is very important for device fabrication and potential commercialization.

Initial OFET device fabrication revealed that films of both BTT-T and BTT-TT annealed at 100 °C performed similarly to the as-cast films (~0.05 cm^2/(V s) and ~0.01 cm^2/(V s), respectively), whereas a significant increase in mobility was observed after applying a 200 °C annealing step for 10 min. For both systems, this behavior is reflected in the UV−vis characteristics of the thin films, as illustrated in Figure 7; the high-energy absorption peak increases relative to the lower-energy absorption peak, which bears more resemblance to a shoulder than a distinct peak after the 200 °C annealing step. This effective blue-shift has been observed previously for other high-performance semiconductors with strong tendencies for aggregation.[2f,g] Although it indicates a decrease in effective conjugation length along the polymer backbone, a favorable reorganization (for example, in the form of H-aggregation, giving rise to stronger intermolecular interactions and higher charge-carrier mobilities) cannot be excluded.[5]

The thin film surface morphologies were studied with close-contact AFM and polarized optical microscopy (POM). The thin film of BTT-T has a fairly homogeneous surface, whereas BTT-TT exhibits a more granular texture with an increase in rms surface roughness from 1.9 nm to 4.0 nm, as illustrated in Figure 8 for the annealed films. In addition, there is a pronounced increase in optical birefringence when moving from BTT-T to BTT-TT films. These data are indicative of an enhanced degree of crystallinity in the BTT-TT polymer. As also observed for poly(3-hexylthiophene),[6] the lower-molecular-weight material (BTT-TT) displays a higher degree of microscopic crystallinity, but a lack of intergrain coherence and connectivity restricts charge carrier mobility on a macroscopic level (see Supporting Information for additional AFM images). Calculations from the subthreshold slopes in Figure 4 estimate that the BTT-TT film has a trap density of (5.0 ± 0.4) × 10^{12} cm^{-2} eV^{-1}, compared to

dx.doi.org/10.1021/cm2015884 |*Chem. Mater.* 2011, 23, 4025–4031

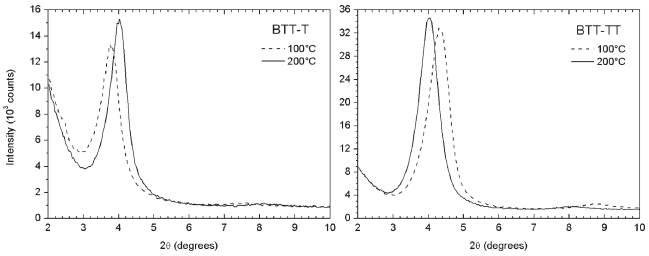

Figure 9. X-ray diffraction (XRD) patterns of drop-cast films of BTT-T (left) and BTT-TT (right) on Si/SiO_2 substrates annealed at (- - -) 100 °C and (—) 200 °C for 10 min under nitrogen.

only $(1.6 \pm 0.3) \times 10^{12}$ cm^{-2} eV^{-1} for the BTT-T device. These energy states are often indicative of intergrain defects, again suggesting a cause of the lower measured mobility in BTT-TT films.

X-ray diffractometry (XRD) was used to probe the bulk morphologies of the polymers. Drop-cast films of BTT-T and BTT-TT were prepared on silicon substrates, and the resulting diffraction patterns are displayed in Figure 9. The BTT-T polymer film displays a significant increase in crystallinity upon annealing at 200 °C, as well as a shortening of the layer-to-layer lamellar distance from 23 Å to 22 Å, as evidenced by the change in the position of the diffraction peak from 3.8° to 4.0°. The tighter packing and higher degree of crystallinity correspond well with the 4−5-fold increase in hole mobility observed upon annealing at 200 °C. BTT-TT, on the other hand, shows much less change in the degree of crystallinity upon annealing, which is in good agreement with the smaller change in FET properties. We furthermore note that the lamellar packing for BTT-TT is, in fact, slightly loosened from 20 Å to 22 Å during the 200 °C annealing step. Distinct diffraction peaks related to $\pi-\pi$ stacking could not be identified for either polymer (see Figure S13 in the Supporting Information for full range diffractograms), which could be explained by the existence of H-aggregates, as discussed above or a preferential orientation of the π-stacks perpendicular to the incident X-ray.

4. CONCLUSIONS

In conclusion, we have successfully incorporated our newly developed benzo[1,2-b:3,4-b′:5,6-d′]trithiophene (BTT) moiety into two novel co-polymers, which show very promising organic field-effect transistor (OFET) performance. We have found the choice of co-monomer to play a crucial role in determining the backbone conformation, the interchain interactions and the polymer solubility. Despite strong aggregation effects and limited solubility, which give rise to fairly low molecular weights, these polymers have hole mobilities exceeding 0.1 $cm^2/(V\ s)$. When also considering the regiorandom nature of the alkyl-bearing BTT unit, this is quite remarkable, highlighting the potential of this building block in semiconductor materials. Finally, we note that further optimization of the balance between solubility and processability versus molecular weight, aggregation, and intermolecular packing is likely to result in improved OFET performances.

■ ASSOCIATED CONTENT

Ⓢ Supporting Information. TGA and DSC traces for both polymers, additional AFM images, XRD spectra, and NMR spectra of all new compounds. This material is available free of charge via the Internet at http://pubs.acs.org.

■ AUTHOR INFORMATION

Corresponding Author

*E-mail: c.nielsen@imperial.ac.uk.

■ ACKNOWLEDGMENT

This work was in part carried out under the EPSRC Project EP/F056710/1, EC FP7 ONE-P 245 Project 212311 and DPI Grant 678, with support from the Centre for Plastic Electronics at Imperial College, the 246 International Collaborative Research Program of Gyeonggi-do, 247 Korea and the National Research Fund of Luxembourg.

■ REFERENCES

(1) (a) Katz, H. E. *Chem. Mater.* **2004**, *16*, 4748. (b) Zaumseil, J.; Sirringhaus, H. *Chem. Rev.* **2007**, *107*, 1296. (c) McCulloch, I.; Heeney, M.; Chabinyc, M. L.; DeLongchamp, D.; Kline, R. J.; Cölle, M.; Duffy, W.; Fischer, D.; Gundlach, D.; Hamadani, B.; Hamilton, R.; Richter, L.; Salleo, A.; Shkunov, M.; Sparrowe, D.; Tierney, S.; Zhang, W. *Adv. Mater.* **2009**, *21*, 1091. (d) Facchetti, A. *Chem. Mater.* **2011**, *23*, 733. (e) Sun, J.; Zhang, B.; Katz, H. E. *Adv. Funct. Mater.* **2011**, *21*, 29.

(2) (a) Garnier, F.; Hajlaoui, R.; Yassar, A.; Srivastava, P. *Science* **1994**, *265*, 1864. (b) McCulloch, I.; Heeney, M.; Bailey, C.; Genevicius, K.; MacDonald, I.; Shkunov, M.; Sparrowe, D.; Tierney, S.; Wagner, R.; Zhang, W.; Chabinyc, M. L.; Kline, R. J.; McGehee, M. D.; Toney, M. F. *Nat. Mater.* **2006**, *5*, 328. (c) Osaka, I.; Abe, T; Shinamura, S.; Miyazaki, E.; Takimiya, K. *J. Am. Chem. Soc.* **2010**, *132*, 5000. (d) Li, Y.; Singh, S. P.; Sonar, P. *Adv. Mater.* **2010**, *22*, 4862. (e) Zhang, W.; Smith, J.; Watkins, S. E.; Gysel, R.; McGehee, M.; Salleo, A.; Kirkpatrick, J.; Ashraf, S.; Anthopoulos, T.; Heeney, M.; McCulloch, I. *J. Am. Chem. Soc.* **2010**, *132*, 11437. (f) Bronstein, H.; Chen, Z.; Ashraf, R. S.; Zhang, W.; Du, J.; Durrant, J. R.; Tuladhar, P. S.; Song, K.; Watkins, S. E.; Geerts, Y.; Wienk, M. M.; Janssen, R. A. J.; Anthopoulos, T.; Sirringhaus, H.; Heeney, M.; McCulloch, I. *J. Am. Chem. Soc.* **2011**, *133*, 3272. (g) Lei, T.; Cao, Y.; Fan, Y.; Liu, C.-J.; Yuan, S.-C.; Pei, J. *J. Am. Chem. Soc.* **2011**, *133*, 6099.

(3) Nielsen, C. B.; Fraser, J. M.; Schroeder, B. C.; Du, J.; White, A. J. P.; Zhang, W.; McCulloch, I. *Org. Lett.* **2011**, *13*, 2414.

(4) (a) Rieger, R.; Beckmann, D.; Mavrinskiy, A.; Kastler, M.; Müllen, K. *Chem. Mater.* **2010**, *22*, 5314. (b) Osaka, I.; Abe, T.; Shinamura, S.; Takimiya, K. *J. Am. Chem. Soc.* **2011**, *133*, 6852.

(5) (a) Scheibe, G. *Angew. Chem.* **1937**, *50*, 212. (b) Menzel, H.; Weichart, B. *Langmuir* **1994**, *10*, 1926. (c) Kim, S.-o.; An, T. K.; Chen, J.; Kang, I.; Kang, S. H.; Chung, D. S.; Park, C. E.; Kim, Y.-H.; Kwon, S.-K. *Adv. Funct. Mater.* **2011**, *21*, 1616.

(6) Kline, R. J.; McGehee, M. D.; Kadnikova, E. N.; Liu, J.; Fréchet, J. M. J.; Toney, M. F. *Macromolecules* **2005**, *38*, 3312.